International Journal of Environmental Science and Technology (2022) 19:2529–2544
https://doi.org/10.1007/s13762-021-03309-y

ORIGINAL PAPER

Assessment and classification of lignocellulosic biomass recalcitrance by principal components analysis based on thermogravimetry and infrared spectroscopy

A. Ramírez-Estrada[1,2] · V. Y. Mena-Cervantes[1,2] · F. S. Mederos-Nieto[1,2] · G. Pineda-Flores[1,2] · R. Hernández-Altamirano[1,2]

Received: 24 July 2020 / Revised: 23 March 2021 / Accepted: 5 April 2021 / Published online: 23 April 2021

Abstract

Lignocellulosic biomass is a high potential feedstock to produce biofuels and value-added products contributing to sustainable bioeconomy. Nevertheless, biomass recalcitrance reduces the yield of processing routes, and therefore, characterization of structural and chemical factors contributing to this resistance must be carried out by robust but rapid and economical analytical techniques. In this work, the recalcitrance of eight lignocellulosic biomass samples: agave bagasse (AB), banana peel (BP), corn cob (CB), barley straw (BS), orange peel (OP), pineapple peel (PP), sugarcane bagasse (SB) and sawdust (SW), was performed infrared spectroscopy and thermogravimetric analysis. The classification of chemical and thermal behavior was based on principal components analysis (PCA) by similarity to four reference materials, cotton fiber (CF), lignin (LG), citrus pectin (CP) and potato starch (PS). The results indicate a clear trend of recalcitrance in four well-defined groups (GPI–GPIV): GPII or lignin-like biomasses (LG and AB) were assessed as the most recalcitrant biomass type (devolatilization temperature: ~ 150 °C, remaining weights > 30wt%), followed by GPI or cellulosic-like biomass (CF, SW and SB), which contain high amounts of cellulose that increase its recalcitrance to thermal degradation (devolatilization temperature: 200–380 °C, remaining weights < 20wt%). GPIII or pectin-like biomasses (CP, PP, OP, BP), known to be significant sources of pectin and hydrolyzable polysaccharides, were classified as intermediated recalcitrance biomasses (devolatilization temperature: 150–350 °C, remaining weights < 30%wt,), whereas GPIV or starchy-like biomasses (PS, BS and CB) were the least recalcitrant materials (devolatilization temperature: 250–350 °C, remaining weights < 30 wt%). This methodology could be applied to classify novel uncharacterized lignocellulosic biomasses irrespectively of their origin based on their similarity to reference materials and to preselect the processing route, to biofuels or biomaterials, in a fast and economical manner.

Editorial responsibility: Josef Trögl.

✉ V. Y. Mena-Cervantes
nymena@gmail.com

[1] Centro Mexicano para la Producción más Limpia, Instituto Politécnico Nacional, Av. Acueducto s/n, Col. La Laguna Ticomán, 07340 Ciudad de México, México

[2] Laboratorio Nacional de Desarrollo y Aseguramiento de la Calidad de Biocombustibles (LaNDACBio), Instituto Politécnico Nacional, 07340 Ciudad de México, México

Graphic Abstract

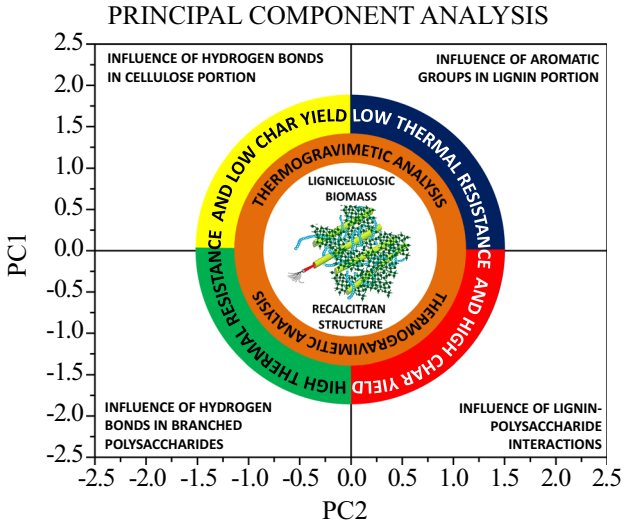

Keywords Lignocellulosic biomass · TGA · FTIR · Recalcitrance · Biomass processing · Biofuels

Abbreviations

LCB	Lignocellulosic biomass
TGA	Thermogravimetric analysis
FTIR	Fourier transform infrared
IR	Infrared
TG	Thermogram
DTG	Differential thermogram
PCA	Principal component analysis
PCI	Principal component one
PCII	Principal component two
PCIII	Principal component three
GPI	Group one
GPII	Group two
GPIII	Group three
GPIV	Group four
AB	Agave bagasse
BP	Banana peel
BS	Barley straw
CP	Citrus pectin
CB	Corncob
CF	Cotton fiber
LG	Lignin
OP	Orange peel
PS	Potato starch
PP	Pineapple peel
SB	Sugarcane bagasse
SW	Sawdust

Introduction

The vegetal biomass is the organic matter from plants that is produced through photosynthetic processes. It can be used to obtain thermal energy, renewable electricity and biofuels, or as a chemical feedstock for bio-based products. A considerable proportion of biomass is lignocellulose (Bar-On et al. 2018), which is mainly compounded by cellulose (40–50%), hemicellulose (25%) and lignin (25%) (Anwar et al. 2014) interlinked in a heterogeneous matrix constituting the plant cell wall, being the sum of the first two components considered as a potential source of carbohydrates.

Lignocellulosic biomass (LCB) has recently gained considerable interest as a high potential resource for the bioenergy industry as some studies have reported a global potential of $8–50 \times 10^9$ tons/year (Al-Battashi et al. 2019), from which a significant percentage is related to crop residues and therefore does not compete with human food supply. In Mexico, for example, approximately 76×10^6 tons of crop residues are generated every year (dry matter), from which 79% is primary waste (such as corn stover, stems of sorghum, leaves of sugarcane, wheat straw, barley straw, bean straw and cotton husk) and the 21% is secondary obtained from post-harvest processing (such as sugarcane bagasse, corncobs, maguey and agave bagasse) (Valdez-Vazquez et al. 2010, Rios and Kaltschmitt 2013). Most of

the agro-industrial biomass is used for animal feeding, but a significant part is burnt in fields (Carrillo-Nieves et al. 2019).

However, LCB displays recalcitrance, which is the natural resistance of plant cell walls to microbial and enzymatic deconstruction, resulting from millions of years of plant evolution to withstand external attacks such as animals, microorganisms and environmental conditions (Melati 2019). This resistance includes those features that limit the biodegradation of biomass such as low reactivity, insolubleness, high thermal stability and/or low available surface area for enzymatic degradation. In general, these aspects can be divided for their study into chemical and structural factors, such as cellulose crystallinity, cellulose specific surface area, degree of polymerization, pore size and chemical composition such as content of cellulose, lignin, hemicelluloses and acetyl groups, respectively (Zoghlami et al. 2019). Thus, recalcitrance is not a direct function of chemical composition only but also of spatial distribution and chemical bonding among the different constituents (Zhao et al. 2012).

Since recalcitrance is often related to heterogeneous distribution of lignocellulosic components (cellulose, hemicellulose and lignin), high lignin content, the crystalline nature of cellulose, high degree of polymerization, as well as covalent linkages between polysaccharides and lignin, the complete characterization of LCB is not trivial, and it requires the use of several techniques which are time-consuming and expensive. Usually, the ASTM E1758-01 and NREL/TP-510–42,618 methods are used to quantify both polysaccharides and lignin, whereas the distribution of lignocellulosic components and their crystallinity often is characterized by infrared (IR) techniques (Xu et al. 2013), Raman spectroscopy, solid-state nuclear magnetic resonance spectroscopy (solid-NMR) (Pereira et al. 2016), X-ray diffraction or imaging analysis (Karimi and Taherzadeh 2016); the covalent linkages between lignin and polysaccharides have been studied by solid-NMR; the surface morphology, particle size, particle shape, particle dimensions and lignocellulose microstructure have been analyzed by scanning electron microscopy (SEM), transmission electron microscopy (TEM) and atomic force microscopy (AFM). Moreover, the combination of SEM with energy-dispersive spectroscopy (EDS) can be used in the elemental analyses of lignocellulosic particles. Therefore, there is a necessity for developing a robust but accessible and fast methodology to characterize both structural and chemical recalcitrance aspects of lignocellulosic biomass.

In this context, Fourier-transformed infrared spectroscopy (FTIR) is a type of molecular vibrational spectroscopy that detects the absorbance of chemical functional groups. This technique has been widely used to detect biomolecules (i.e., lipids, carbohydrates, amino acids, triglycerides, fatty acids, etc.), to identify functional groups associated to the lignocellulosic structure and to elucidate changes in biomass structure after pre-treatment (Lupoi et al. 2014).

Shah et al. 2018 evaluated the presence of cellulose, hemicelluloses and lignin of different walnut shells by FTIR for their potential use as biofuels. Characteristic bands of such lignocellulosic biomass were located at ~ 3400 cm^{-1} corresponding to O–H stretching vibration; prominent peaks were obtained at ~ 3030 cm^{-1}, which represent the C–H stretching vibrations for aromatics in lignin. The bands at 1740 cm^{-1} corresponding to the C=O esters of acetyl group in the hemicelluloses fraction were also observed. Peak at 1510 cm^{-1} indicated aromatic C=C ring stretching vibration in lignin. The medium-intensity band at ~ 1430 cm^{-1} was assigned to the aromatic C=C ring stretching vibration in lignin, whereas the band between 1060 and 1030 cm^{-1} corresponding to C–O stretching confirmed the presence of aliphatic ether or alcohol from cellulose, hemicellulose and lignin.

Rodier et al. 2019 used FTIR to evaluate the change in the content of polysaccharides and lignin of sugarcane bagasse and its derived biochar. They observed that the thermochemical processing caused a decrease in the intensity of all the signals except for the one located at ~ 3030 cm^{-1}, corresponding to the vibration of elongation of the aromatic C-H bond. FTIR analysis of biochar (pyrolysis product) indicated that thermochemical conversion process of sugarcane bagasse affects more to the polysaccharide fraction.

On the other hand, the thermogravimetric analysis (TGA) has been used to characterize the thermal decomposition of lignocellulosic biomass such as sawdust (Mishra et al. 2018) and also to rapidly estimate the proximate composition (García et al. 2013) or the polysaccharide content of lignocellulosic biomass. Carrier et al. 2011 found that TGA could be used to determine the α-cellulose and hemicellulose amounts in a biomass sample. They observed successful correlations between the component contents determined from chemical methods and TGA for those structural polysaccharides, but the correlation was not useful to estimate lignin content.

Olatunji et al. 2018 revised thermogravimetric characterization of biomass properties. They conclude that TGA would provide a fast, accurate and efficient technique to determine the utilization of biomass, particularly when is used in combination with other analytical methods, eventually leading to a robust modeling tool, that could be used to determine the utilization of biomass irrespective of its nature.

TGA-FTIR tests have been applied to study the volatilization of lignocellulosic biomass such as almond and hazelnut shells, sunflower stalk (Ballice et al. 2020) and wheat straw (Ramezani, 2018). However, these results have not been used to characterize the recalcitrance of such organic materials in order to classify different types of biomass sources or to systematize the selection of processing routes based on the degree of recalcitrance.

In this context, principal component analysis (PCA) is a statistical tool that enables identifying groups of variables behaving similarly in a complex data set. It has been previously used to discriminate pyrolysis and gasification products from biomass

and also to examine the influence of biomass macromolecular composition on its behavior in torrefaction. In previous studies, spectroscopic and thermogravimetric data were associated with multivariate techniques for the fast characterization of biomass samples towards energetic use. Liu et al. 2016 applied FTIR associated with PCA to evaluate the differences in the accumulation of carbohydrates among cotton plant biomass samples. Lazzari et al. 2018 used FTIR combined to PCA classify fifteen biomass samples through the composition of their bio-oil into three well-differentiated groups. Such clustering information allowed exploring bio-oil quality prior to the pyrolysis process. Ohraaho 2013 applied PCA based on analytical pyrolysis-GC/MS data to study the influence of lignin substructures of eighteen Eucalyptus species on the composition of pyrolysis products and tried to classify the studied samples into four categories based on the chemical composition of pyrolyzate. Gil et al. (2019) applied PCA on physicochemical variables from the gasification process of ten LCB samples to study the influence of the biomass characteristics on this thermochemical process. They found a clear separation of the biomass samples into two main groups based on the gasification results. Gonzalez et al. 2020 analyzed the information from torrefaction process of fourteen woody and agricultural biomass samples using PCA to assess the influence of biomass macromolecular composition on its behavior in torrefaction. Their results indicated that it is possible to group biomass samples based on the production of volatile components.

Thus, previous reports show that multivariate analysis techniques, such as PCA, can be applied to data from fast but robust analytical methods having a high potential to be used as an analysis tool for the study of biomass recalcitrance. In this context, PCA can be applied to analyze chemical and structural information provided by TG and FTIR analysis of lignocellulosic biomass to classify the grade of its recalcitrance and further systematize the selection of processing routes. To our best knowledge, this is the first report on the application of PCA based on thermogravimetric and spectroscopic information from lignocellulosic biomass to characterize the recalcitrance response from structural and chemical factors as a tool to classify raw biomass sources and to systematize the selection of the more suitable processing route for sources of LCB.

In the present study, FTIR spectroscopy and TGA were used to assess the structural and chemical recalcitrance of eight different types of biomass samples: agave bagasse (AB), banana peel (BP), corn cob (CB), barely straw (BS), orange peel (OP), pineapple peel (PP), sugarcane bagasse (SB) and sawdust (SW), where four of them were taken as reference materials corresponding to cellulose-rich (cotton fiber), lignin-rich (lignin, LG), polysaccharide-rich (citrus pectin, CP) and starchy biomass (potato starch, PS). The results were analyzed through PCA to classify lignocellulosic biomasses according to their similarity to reference materials and used to select a biochemical or thermochemical processing route for a given biomass sample. This approach would be used to classify LCB recalcitrance of novel biomass samples irrespective of their source nature and to preselect the best conversion route based on the data known for the reference material with the highest similarity.

Materials and methods

Biomass samples

Twelve types of biomasses, namely cotton fiber (CF), potato starch (PS), citrus pectin (CP), sawdust (SW), sugarcane bagasse (SB), corncob (CB), barley straw (BS), orange peel (OP), pineapple peel (PP), banana peel (BP), agave bagasse (AB) and lignin (LG), were used for experimentation. The CF used was surgical grade, while that PS (from JT. Baker ACS), AP (from Sigma-Aldrich), CP (from Sigma-Aldrich) and LG (from Sigma-Aldrich) were reagent grade. The CB, BS and AB (*A. salmiana gentry*) were collected in Santa Teresa Tlaxcala MX (19°32′30″N and 98°36′26″W at 2756masl). The SB, OP, PP and BP were collected from nearby fruits stall of Zacatenco Gustavo A. Madero CDMX (19°30′15″N and 99°07′32″W at 2241masl). The raw materials (about 20 g) were washed with deionized water, oven-dried at 85 °C for 4 hr, powdered, sifted through a 12-mesh sieve and oven-dried at 85 °C for 4 hr. All the samples were collected in the period of March to June, 2020.

TGA measures

TGA measures were carried out in a Perkin-Elmer STA-6000 instrument. The sample (about 100 mg) was placed into an alumina sample pan and heated from 30 to 600 °C at a rate of 10 °C•min^{-1} under inert atmosphere (supplying nitrogen at 20 ml·min^{-1}); the sample was preheated at 105 °C and kept isothermal conditions by 5 min prior TGA measures to remove moisture according to the previous report from Munir et al. 2009. The sample weight was continuously recorded as a function of the temperature and time using the Pyris software (version 13.3.1.0014). Likewise, derivative thermogravimetric analysis (DTG) was carried out to portray the weight loss of the sample with respect to the temperature. The TGA measures were performed by triplicate using the same operating conditions to establish the reproducibility of the data.

Principal component analysis

Principal component analysis (PCA) is a dimension reduction technique by linear combination of the original variables into different principal components. It is a nonparametric method useful for obtaining relevant information from a complex data set.

PCA was performed on the TG-results using the OriginPro 2018 software. The complete data set, defined by the variables in the columns (in this study, 27,710 temperatures) and the %weight samples in the rows, was autoscaled through mean centering by column. PCA models the maximum directions of variation in a data set by projecting the objects (i.e., the TG-curves) as a whole of points in a space defined by principal components.

Heating experiments and char characterization

Heating experiments and infrared analysis were carried out to analyze the functionality alterations during the heating process. The samples were heated to analyze the functionality alterations during the heating process. The heating experiments were carried out in a Perkin-Elmer STA-6000 instrument. The sample (about 200 mg) was heated in an alumina sample pan from room temperature (~28 °C) to 600 °C at a rate of 10 °C•min^{-1} under inert atmosphere (supplying nitrogen at 20 ml·min^{-1}). The sample temperature controller was turned off depending on which final temperature was investigated, and the sample pan was allowed to cool with a small N_2 purge. Once the sample pan had cooled, the remnant residue was collected and analyzed by FTIR to identify the functional groups. IR spectra were recorded with a Perkin-Elmer Frontier FTIR spectrometer equipped with a diamond attenuated total reflectance (ATR) accessory. The spectra were obtained using 32 scans in the 4000–600 cm^{-1} range at a resolution of 4 cm^{-1}.

FTIR analysis

IR spectra were recorded with a Perkin-Elmer Frontier FTIR spectrometer equipped with a diamond attenuated total reflectance (ATR) accessory. The spectra were obtained using 32 scans in the 4000–600 cm^{-1} range at a resolution of 4 cm^{-1}. The crop residues and fruit wastes were dried at 80 °C by 8 h and milled up < 2 mm, prior FTIR analysis. Meanwhile, CF, PS, CP and LG were analyzed without pre-treatment.

Results and discussion

TGA of reference materials

Figure 1 shows the thermogravimetric (TG) and differential thermogravimetric (DTG) curves of reference samples (cotton fiber, potato starch, citrus pectin and lignin); the complete experimental data are provided in Table S1. CF shows a drastic weight loss (~82%) at 250–380 °C range. In addition, DTG curve of CF shows a sharp peak at ~365 °C, which represents the primary devolatilization of the cellulosic portion as observed by Yang et al. 2007 and Abidi et al. 2010a. Cabrales et al. 2010 and Brillard et al. 2017 found that the devolatilization of cotton fiber begins at high temperatures (T > 250 °C) within a narrow temperature range (315–400 °C), producing a high quantity of volatile compounds (about 80%) and low char yields (< 10%).

PS-TG curve shows a sharp weight loss (~75%) in the range of 270–400 °C. Besides, DTG-PS curve shows a single peak at 294 °C and a small shoulder on the high-temperature side. Some authors have studied the thermal decomposition of starches using TGA methods; Rudnik et al. 2006 studied the thermal behavior of different starch derivatives and found that the higher degradation is below 300 °C. Liu et al. 2010 found that the thermal stability of corn starches

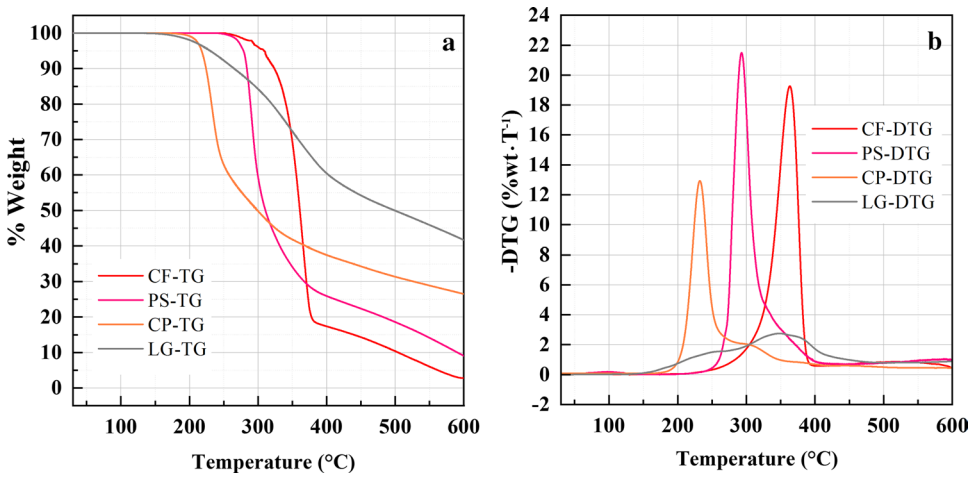

Fig. 1 TGA profile of reference samples in dry base; **a** TG curves and **b** DTG curves

decreased with increase in amylose content; Lemos et al 2019 found that DTG at ~ 300 °C is attributed to dissociation of the amylose chains, whereas 365 °C corresponded to amylopectin degradation, being both biopolymers the main constituents of starchy-like biomasses. On the other hand, CF-DTG and PS-DTG curves show a single peak and the main thermal decomposition of PS takes place at lower temperatures (between 180 and 350 °C). This behavior suggests that the thermal degradation of CF and PS is influenced by the microstructure; the PS is composed of branched polysaccharides, while that CF is composed of crystalline cellulose.

CP-TG curve shows a weight loss step in the range of 190–290 °C followed by a change in the slope leading to a lower weight loss. In addition, CP-DTG shows a single wide-peak in the range of 190–290 °C and a small shoulder on the high-temperature side. Fisher et al. 2002 reported that pectin decomposes very quickly around 250 °C. Einhorn-Stoll et al. 2007 found that the pectin degrades at temperature range between 210 and 270 °C. Aburto et al. 2015 performed a non-isothermal kinetic analysis of pectin pyrolysis to understand the pyrolysis of citrus peel. This study suggests that the pyrolytic degradation of pectin is a complex set of simultaneous and consecutive reactions related to (1) initial depolymerization by breaking the glycosidic linkages ($T \leq 200$ °C), (2) secondary degradation of pectin units (between 250 and 580 °C) and (3) direct gasification of char residues ($T \geq 600$ °C).

LG-TG curve shows a continuous weight loss from 150 °C until 700 °C. Likewise, LG-DTG curve shows a shoulder on the low-temperature side (between 150 and 300 °C) as well as a wide-peak at ~ 350 °C. The degradation of LG is slower from 475 °C, and the weight decreases gradually as temperature increases. Besides, a large amount (about 41%) of LG remains unvolatilized at 600 °C. The thermal degradation of lignin occurs over a broad temperature range because the functional groups from its structure have different thermal stabilities (Park et al. 2018). The lignin degradation process involves fragmentation of inter-unit linkages (between 200 and 300 °C), releasing of monomers and derivatives of phenol units (between 300 and 450 °C), and degradation of polycyclic aromatic compounds ($T > 450$ °C) as observed by Brebu et al. 2013 and Kawamoto 2017.

The main devolatilization (i.e., weight loss) of the samples of FC and LG is observed between 200 and 400 °C and the degradation of CF begins at higher temperatures (> 250 °C); due to the stability of the hydrogen bond network and stacking forces between cellulose fibers (Abidi et al. 2007). On the other hand, the devolatilization of CF is higher than LG as temperature increase (> 345 °C); the degradation of LG decreases as increase the temperature due to the formation of high condensed aromatic structures (Brebu et al. 2013). Both PS and CF are composed of long polymer chains of glucopyranose units and the weight loss of CF and PS at 300 °C was ~ 6 and ~ 42 wt%, respectively. This difference could be related to differences in the degree of polymerization and branching as the starch is less ordered and of much lower molecular weight than cellulose of CF.

TGA of lignocellulosic samples

Figure 2 shows the thermograms (TG) and differential thermogravimetric (DTG) curves of lignocellulosic samples; the complete experimental data are provided in Table S1. In general, the thermal degradation of lignocellulosic materials involves three stages of decomposition (Dhyani and Bhaskar 2018); the first stage (between 150 and 220 °C) comprises the decomposition of light compounds (such as waxes, organic acids, oils, terpenes or pigments); the second stage (between 220 and 380 °C) comprises the decomposition of polymeric structures; and the third stage (between 380 and 600 °C) involves the direct gasification of the heaviest organic compounds.

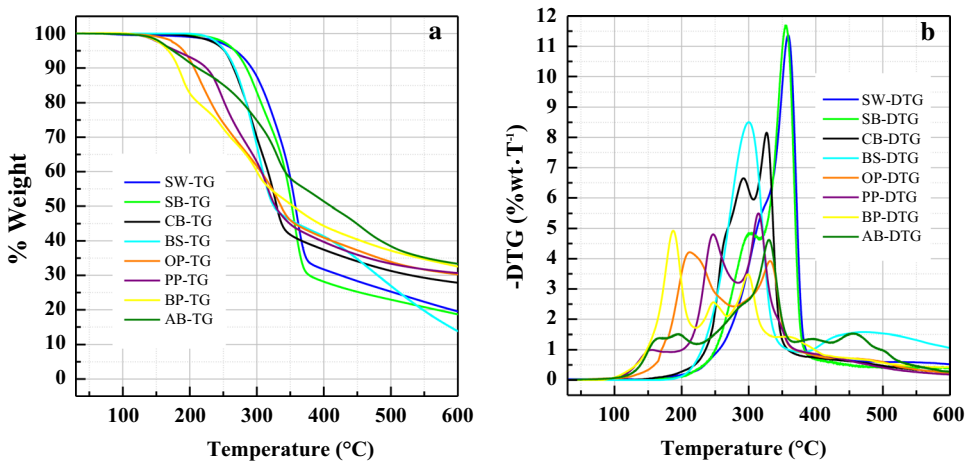

Fig. 2 TGA profile of lignocellulosic samples in dry base; **a** TG curves and **b** DTG curves

The curves WO-DTG, SB-DTG and CB-DTG show two overlapping peaks, in the range of 220–380 °C, which denotes a superposition of hemicellulose and cellulose degradation; the devolatilization of hemicellulose and cellulose takes place at a very close temperature range so that there is an overlapping of their degradation zone and usually two distinct peaks can be observed in the DTG curve (Yang et al. 2007, 2011). AB-TG curve shows a continuous weight loss from 150 °C until 600 °C. Moreover, the AB-DTG curve shows multiple peaks of decomposition in the ranges of 100–150 °C.

PCA results

Figure 3 shows the plot score for the first three principal components (PC1, PC2 and PC3); these components account for 87.5% of the total variance of the data. Likewise, Fig. S1 shows the loading plot for the first three principal components (see supplementary material); the negative side of PC1 (–PC1-axis) denotes moderate devolatilization (i.e., weight loss) between 120 and 350 °C, and the positive side (+PC1-axis) denotes high residual weights between 350 and 600 °C; the negative side of PC2 (–PC2-axis) denotes low devolatilization between 30 and 180 °C and the positive side (+PC2-axis) denotes moderate devolatilization between 180 and 300 °C as well as low residual weights between 375 and 600 °C; the negative side of PC3 (–PC3-axis) denotes low devolatilization in the range of 95–275 °C as well as high devolatilization between 360 and 600 °C, while that the positive side (+PC3-axis) denotes devolatilization between 275 and 360 °C.

Relation between functional groups and thermal degradation

Figure 4 shows the PC1 vs PC2 score plot. This plot shows a clear separation of the samples (i.e., scores) into four groups; Group I (GPI) includes CF, SW and SB; Group II (GPII) includes LG and AB; Group III (GPIII) includes CP, BP, PP and OP; Group IV (GPIV) includes PS, BS and CB. Likewise, Table 1 summarizes the onset temperature degradation (T_o), number of step, step temperature (T_i), step percent weight ($\%wt_i$) and step percent weight at 600 °C ($\%wt_{600\,°C}$).

The samples of GPI are on the –PC1-axis and +PC2-axis. In this group, the main devolatilization (i.e., the main weight loss step) of the samples is between 200 and 380 °C, and the remaining weight is lower than 20%. Figure 5 shows the IR spectrum of both CF and resultant char. CF is a material composed of cellulose (about 98–99%) with some non-cellulosic components (such as waxes or proteins) surrounding the cellulose core (Hersh et al. 2006). In addition, the cotton fiber spectrum (CF-IR) shows a broad absorption band in the range of 3640–3000 cm^{-1} (O–H stretching vibration arising from intra-molecular hydrogen bonding in cellulose), two small absorption bands at 3000–2755 cm^{-1} (–CH–stretching vibration), little absorption bands at 1688–1500 cm^{-1} (C=O and NH_2 vibration from amide) (Abidi et al. 2014), small absorption bands at 1500–1190 cm^{-1} (C–H, C–C or C–O asymmetric stretching vibrations) and strong overlapped-adsorption bands at 1190–840 cm^{-1} (C–OH, C–O stretching of pyranose rings and C–O–C vibration of glycosidic linkages) (Chung et al. 2004; Abidi et al. 2010b). The cellulose is a linear polysaccharide composed entirely of β-(1–4) linked D-glucose units. Besides, the –OH groups in each monomeric unit can interact with one another to form intra- and inter-molecular hydrogen

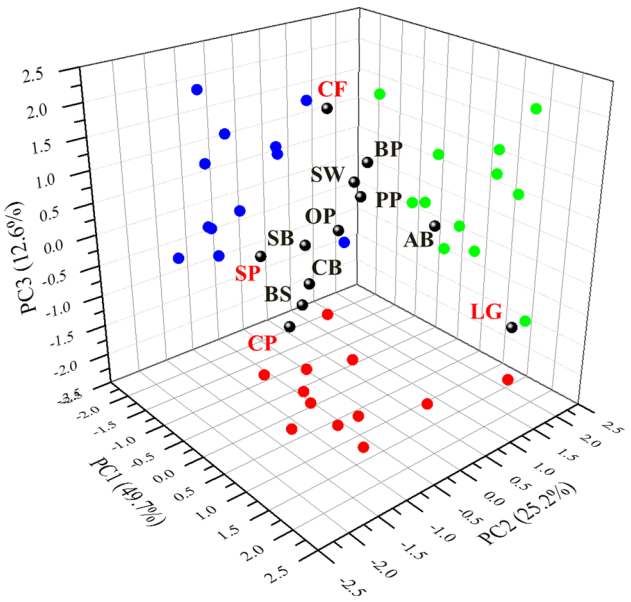

Fig. 3 Score plot of the three first principal components

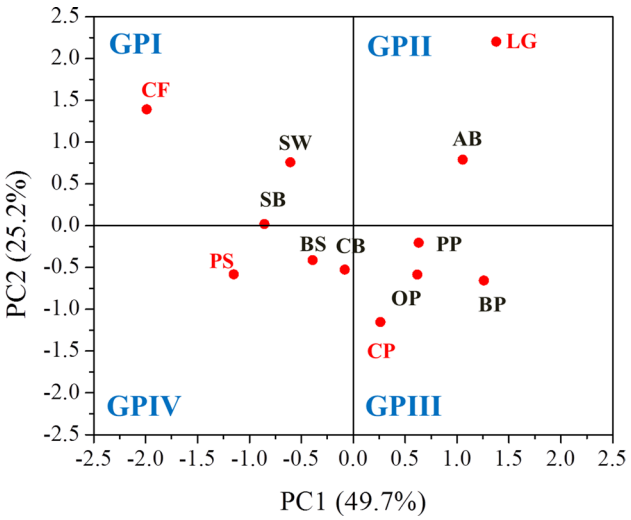

Fig. 4 Score plot of the two first principal components

Table 1 Thermogravimetric analysis trends for GPI–GPIV biomasses

Group	Sample	No. steps	Temp. range	150–200 °C		200–250 °C		250–300 °C		300–325 °C		325–400 °C		400–450 °C		450–500 °C		$\%wt_{600\,°C}$
			T_o (°C)	T_{max} (°C)	%wt	T_{max} (°C)	%wt	T_{max} (°C)	%wt	T_{max} (°C)	%wt	T_{max} (°C)	%wt	T_{max} (°C)	%wt	T_{max} (°C)	%wt	
GPI	CF	1	235.8									364.8	42.5					1.8
	SW	2	175.6							321.3	78.2	353.1	55.7					19.5
	SB	2	170.2							302.5	82.3	353.7	49.4					18.7
GPII	LG	3	145.6			249.9	92.1					347.2	73.5	426.9	57.8			41.1
	MY	7	124.9	162.4	96.7	202.3	92.4	288.1	77.8			330.0	64.8	397.9	51.7	455.9	44.0	33.4
GPIII	PC	2	184.1			231.5	80.9			300.0	51.2							26.5
	PP	4	128.5	155.8	97.2			250.1	80.7	313.6	56.7			419.4	38.1			30.7
	OP	6	144.5	199.6	89.9	232.4	79.8			294.5	62.9	331.9	51.7	402.1	40.8	467.5	36.0	30.3
	BP	5	122.4	186.2	88.4			249.3	72.6	297.5	60.9	363.9	48.6	440.4	40.9			32.6
GPIV	SP	1	217.9							293.4	21.16							11.0
	CB	3	123.7					226.2	98.4	293.7	73.9	326.4	53.8					27.8
	BS	2	187.8							299.7	67.8					473.5	31.1	13.8

To = onset temperature of decomposition T_{max} = Temperature of decomposition in the step wt% = Percent weight in the step $wt\%_{600\,°C}$ = Percent weight at 600 °C

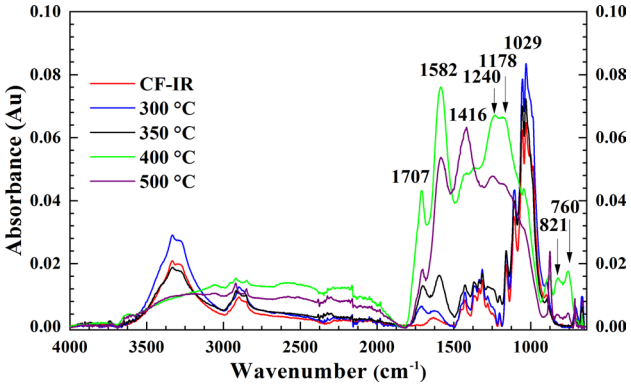

Fig. 5 IR spectra of CF and the chars collected at different temperatures

bonds, leading to ordered (i.e., crystalline) structures (Abidi et al. 2010b). In turn, the hydrogen bonds of cellulose chains enhance the thermal stability of the CF structure. The thermal degradation of cellulose involves reactions of dehydration, depolymerization, ring-opening, decarboxylation and charring (Xin et al. 2015; Liang et al. 2018). Dehydration is the favored reaction at low temperatures (< 300 °C); this process involves the dissociation of inter-hydrogen bonds by the elimination of –OH groups as well as the formation of anhydrocellulose. At 200 °C, the biochar spectrum shows absorption bands in the ranges of 3640–2750 cm^{-1}, 1500–1190 cm^{-1} and 1190–840 cm^{-1}, which confirm the formation of anhydrocellulose. The degradation of anhydrocellulose proceeds through intra-molecular condensation (i.e., dissociation of intra-hydrogen bonds) and depolymerization to form small-molecular-weight compounds (such as H_2O, CO_2, CO, levoglucosan and HMF) (Lin et al. 2009). The spectrum of the chars collected at 350 °C shows absorption bands in the range of 1750–1500 cm^{-1} (C=O vibrations of acetyl, ester, carboxyl groups as well as C=C vibrations of ethylene groups); these bands resulted from partial degradation of anhydrocellulose. The anhydrocellulose structure breaks down at temperatures higher than 400 °C. For example, the spectrum of the char collected at 400 °C and 500 °C shows two strong absorption band at ~ 1582 (C=C vibrations of aromatic groups) cm^{-1} and ~ 1416 cm^{-1} (C–H_2 and CH_3 bending vibration of aliphatic groups). Moreover, these spectra show an increasing upward-drift in the baseline between 3700 and 1800 cm^{-1}. Therefore, the degradation of CF is slower at high temperatures (> 380 °C) due to the formation of polyaromatic structures.

Figures S2-S3 show the IR spectrum of SW and SB as well as the spectrum of resultant biochars (supplementary material). SW-IR and SB-IR spectrum shows absorption bands in the ranges of 3600–2700 cm^{-1} (O–H stretching vibration of –OH groups, as well as C–H vibrations of methyl and methylene groups) and 1200–900 cm^{-1} (vibrations of C–OH, C–O and C–O–C bonds). Also, these spectra show

small absorption bands in the range of 1750–1500 cm^{-1} (C=O vibrations of acetyl, ester, carboxyl groups as well as C=C vibrations of aromatic groups), which represents the vibrations of functional groups in both hemicellulose and lignin portion (Huang et al. 2012; Santoni et al. 2015; Pereira et al. 2016). The spectra of char-200 °C show absorption bands between 3600 and 3000 cm^{-1} (O–H stretching vibration of –OH groups) and 1200–900 cm^{-1} (vibrations of C–OH, C–O and C–O–C bonds); these bands denote the formation of anhydrocellulose. The spectra of char-400 °C show strong absorption at ~ 1700 cm^{-1} (C=O vibrations of acetyl and ester groups), ~ 1590 cm^{-1} (C=C vibration of aromatic groups) and ~ 1190 cm^{-1}(C–OH vibration of phenolic group). Also, these spectra show an increasing upward-drift in the baseline between 3700 and 1800 cm^{-1}. The weight loss in the ranges of 200–380 °C and 380–600 °C was ~ 70% and ~ 15%, respectively. Then, the degradation of SW and SB is more intense in the range of 200–380 °C due to high reactivity of anhydride cellulose. In contrast, the degradation of SW and SB is slower at high temperatures (> 380 °C) due to the formation of polyaromatic structures.

The samples of GPII are on the + PC1-axis and + PC2-axis. In this group, the devolatilization of the samples begins at lower temperatures (~ 150 °C), and the remaining weight is higher than 30 wt% Figure 6 shows the IR spectrum of both LG and resultant char. LG is a complex aromatic heteropolymer composed of p-hydroxyphenyl, guaiacyl, and syringyl units. In addition, LG-IR shows a broad adsorption band in the ranges of 3670–3010 cm^{-1} (O–H stretching vibration of –OH groups in phenolic structures), 2900–2850 cm^{-1} (–CH– stretching vibration in aromatic methoxyl or methylene groups of side chains), 1700–1650 cm^{-1} (C=O stretching of ketone, carboxyl and ester groups), 1650–1020 cm^{-1} (C–O deformation of ester or ether groups and alcohols, aryl–OH stretching vibration and C–H in-plane deformation) and 880–810 cm^{-1} (C–H deformation of out-plane). The intensity of the bands in the region of 3500–3000 cm^{-1} (O–H stretching vibration of –OH groups) is smaller in the char-350 °C than char-400 °C; this effect could be related to the reactions of dehydration by the dissociation of O–H bonds located to the benzyl group due to the increment of temperature. Meanwhile, the intensity of the bands at 1417 cm^{-1} increased remarkably. Figure S4 shows the IR spectrum of AB and the resultant biochars (supplementary material). The AB-IR spectrum shows absorption bands at 3500–2700 cm^{-1} (O–H and C–H stretching vibration) and 1590 cm^{-1} (symmetric aryl ring stretching vibration). At 400 °C, the biochar spectrum shows a strong absorption band at ~ 1405 cm^{-1}, as well as, an increasing upward-drift between 3500 and 1700 cm^{-1}.

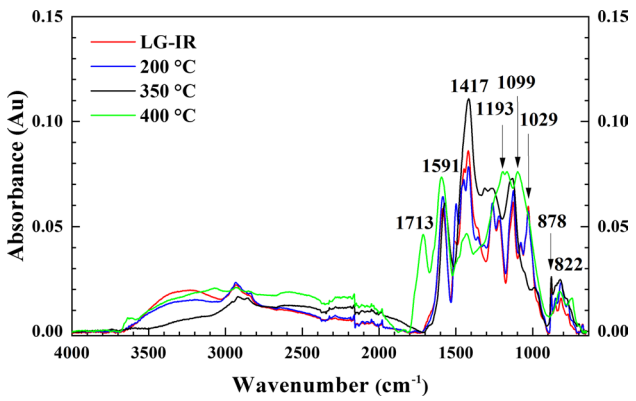

Fig. 6 IR spectra of LG and the chars collected at different temperatures

The main devolatilization (i.e., weight loss) of GPI samples and GPII samples is between 150 and 380 °C. Specifically, the degradation of GPI samples begins at higher temperatures (> 250 °C), indicating that the GPI samples contain a higher amount of recalcitrant components. The IR spectra of CF, SW and SB show absorption bands at 3320 cm^{-1}, 1500–1200 cm^{-1} and 1029 cm^{-1}, which are related to functional groups of cellulose fraction, enhancing the thermal stability of GPI samples. The IR spectra of chars-400 °C show strong absorption at ~ 1592 cm^{-1} (C=C vibration of aromatic groups) and ~ 1410 cm^{-1} (C-H_2 and CH_3 bending vibration of aliphatic groups) related to polyaromatic structures. Then, the devolatilization of GPII samples is slower at high temperatures (> 360) due to the formation of polyaromatic structures.

The samples of GPIII are on the + PC1-axis and -PC2-axis. In this group, the main devolatilization occurs between 150 and 350 °C, and the remaining weights are lower than 30 wt%. Figures S5-S7 show the IR spectrum of fruit wastes (PP, OP and BP) as well as the spectrum of resultant char (see supplementary material). PP-IR, OP-IR and BP-IR spectrum shows absorption bands in the ranges of 3600–3600 cm^{-1} (O–H stretching vibration of –OH groups) and 3000–2700 cm^{-1} (C–H vibrations of methane, methyl and methylene groups). Also, these spectra show small absorption bands in the region of 1780–1500 cm^{-1} (C=O vibration of acetyl, ester, carboxyl groups, as well as, C=C vibration of aromatic groups), as well as, absorption bands between 1180 and 900 cm^{-1} (vibration of C–H, C–C, C–OH and C–O–C bonds). The primary devolatilization of fruit wastes is between 150 and 250 °C. Nevertheless, the IR spectrum of raw material and char-200 °C show similar absorption pattern. The primary devolatilization of fruit wastes is due to decomposition of light compounds (such as waxes, oils, terpenes or pigments). The secondary devolatilization of fruit wastes is between 150 and 350 °C. The IR-char collected at 300 °C shows strong absorption at ~ 1590 cm^{-1} (C=C vibration of aromatic groups). Moreover, the absorption bands at 3500–3000 cm^{-1} (O–H stretching vibration) and 1150–950 cm^{-1} (vibration of C–H, C–C, C–OH and C–O–C bonds) are less intense in char-400 °C

than raw material; its effect could be related to degradation of pectin fraction.

The main devolatilization of GPIII samples and GPI samples occurs between 200 and 380 °C. This behavior could be due to differences in the microstructure or composition; the fruit peels are composed of light compounds and pectin as well as their structure is more flexible than SW and SB. On the other hand, the degradation of both GPIII samples and GPII samples begins at low temperatures (~150 °C). Moreover, the char yield of these samples is higher than 30 wt%. The initial weight loss (in the range of 150–250 °C) of GPIII samples is higher than GPII samples. This means that the organic matter of GPIII samples is more volatile than GPII samples.

The samples of GPIV are on the –PC1-axis and –PC2-axis. In this group, the main devolatilization of the samples is between 250 and 350 °C, and the remaining weights are lower than 30 wt%. Figure S8 shows the IR spectrum of CB as well as the spectrum of resultant biochars (see supplementary material). CB-IR spectrum show absorption bands in the ranges of 3670–3000 cm^{-1} (O–H stretching vibration of –OH groups) and 3000–2780 cm^{-1} (C–H vibrations of methane, methyl and methylene groups). Also, these spectra show small absorption bands in the region of 1775–1511 cm^{-1} (C=O vibration of acetyl, ester, carboxyl groups, as well as, C=C vibration of aromatic groups). The IR spectrum of char collected at 300 and 350 °C shows strong absorbance at 1580, 1395 and 1034 cm^{-1}. Figure S9 shows the IR spectrum of both BS and resultant char (see supplementary material). These spectra show strong absorbance at 1011 cm^{-1} (vibration C–OH and C–O–C bonds) and 792 cm^{-1}. The IR spectrum of biochar-550 °C shows strong absorbance at 1450, 1360 and 960 cm^{-1} (vibration C–OH and C–O–C bonds), as well as, an increasing upward-drift between 3500 and 1700 cm^{-1}.

Analysis of recalcitrance

Figure 7a shows the DTG curves of GPI samples. CF-DTG curve shows a sharp peak at ~365 °C, which represents the devolatilization of the cellulosic portion. Yang et al. (2007) found that the devolatilization of cellulose is at high temperatures (T > 300 °C) within a narrow temperature range (315–400 °C), and the maximum temperature of decomposition is at ~355 °C. On the other hand, SW-TG and SB-TG curves show a sharp weight loss (~67 wt%) in the range of 220–380 °C. Meanwhile, SW-DTG and SB-DTG curves show a wide-peak the range of 330–380 °C as well as a shoulder on the low-temperature side; this shoulder often is related to the primary devolatilization of hemicellulose portion (Mishra and Mohanty 2018a, b; De Palma et al. 2019). Yang et al. (2011) and Zhao et al. (2018) studied the thermal decomposition of several cellulose/hemicellulose/lignin mixtures. They found that the DTG increases with the cellulose proportion and the DTG peak between 320 and 380 °C is related to the decomposition of the cellulose. The highest degradation step for CF, SW and SB is between 220 and 380 °C, and the maximum DTG value is at ~360 °C. This result suggests that CF, SW and SB have a high concentration of cellulose. Since cellulose molecules have a strong tendency to form intra and intermolecular hydrogen bonds, leading to highly ordered (i.e., crystalline) structures; the thermal recalcitrance of SW and SB is originated by the crystallinity of cellulose.

Figure 7b shows the DTG curves GPII samples and CF. DTG curve of LG shows a shoulder on the low-temperature side (between 150 and 280 °C) as well as a wide-peak at ~350 °C, revealing two stages of thermal decomposition. Moreover, the degradation of LG becomes slower at temperatures higher than 500 °C due to polyaromatic structures. AB-DTG curve shows multiple peaks of decomposition in the range of 150–600 °C. Yang et al. (2011) and Zhao et al. (2018) found that the lignin hiders the devolatilization of cellulose as the peak of cellulose degradation decreases due to the presence of lignin and that

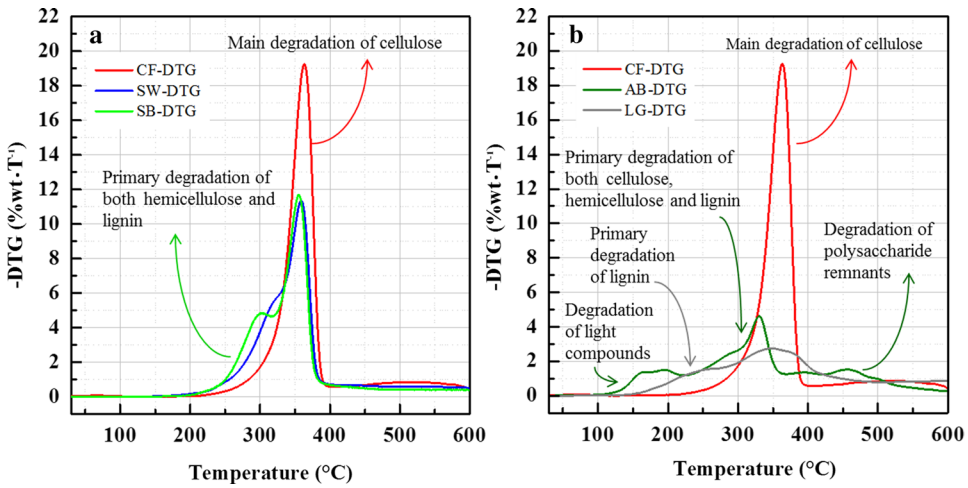

Fig. 7 DTG curves of samples of GPI and GPII

the maximum decomposition rate is slightly shifted towards lower temperatures. The main peak of the DTG curve of AB is between 220 and 350 °C, and this peak is smaller than the CF. Moreover, the IR spectrum of AB-char collected at 300 °C shows strong absorption at 1600 cm^{-1} (C=C vibration of aromatic groups) and 1035 cm^{-1} (vibration of C–H, C–C, C–OH and C–O–C bonds); the absorption band at 1035 cm^{-1} could relate to the vibration of glycoside linkage of polysaccharide units. Its behavior suggests a partial decomposition of polysaccharide portion. The DGT curve for AB shows a small peak at ~ 455 °C, which represents the degradation of remaining polysaccharides; the IR spectrum of AB-char collected at 400 °C shows small absorption at 1053 cm^{-1} (vibration of C–H, C–C, C–OH and C–O–C bonds) relating to moieties of polysaccharide. Then, the thermal recalcitrance of AB is controlled by the presence of lignin.

Figure 8a shows the DTG curves of GPIII samples and CF. The DTG curve of fruit wastes (i.e., PP-DTG, OP-DTG and BP-DTG curves) shows the two highest peaks of decomposition in the ranges of 150–270 °C and 270–350 °C; the first of ones could be relating to the primary degradation of pectin; the second peak could be relating to the decomposition of cellulose. The DTG peaks of fruit wastes are smaller than both CP and CF; this effect could be relating to the bonds between polysaccharides and lignin (i.e., presence of lignin–carbohydrate complexes). The fruit waste spectra (i.e., PP-IR, OP-IR and BP-IR) show strong absorption at ~ 1710 cm^{-1} (C=O vibration of both ester and carboxyl groups) and ~ 1580 cm^{-1} (C=C vibration of aromatic groups); these absorption bands correspond to the ester linkages between lignin and carbohydrates (Giummarella et al. 2013). The thermal decomposition of fruit wastes is slower at temperatures higher than 350 °C. Moreover, the bands at ~ 1710 cm^{-1} and ~ 1580 cm^{-1} are more intense at 400 °C (see IR spectrum of char-400 °C in supplementary material). This behavior suggests that devolatilization of fruit wastes becomes slower due to the stability of lignin–carbohydrate linkages. Then, the recalcitrance of fruit wastes of GPIII is controlled by the bonding between polysaccharides and lignin.

Figure 8b shows the DTG curves of GPIV samples and CF. PS-DTG and CF-DTG curves show a peak at 294 °C and 365 °C, respectively. The peak at 294 °C is attributed to dissociation of the amylose chains, whereas 365 °C corresponded to amylopectin degradation, being both biopolymers the main constituents of starchy-like biomasses (Lemos et al. 2019).

Preliminary selection of processing route

The results from previous sections permit the classification of the eight biomass samples into four well-defined groups regarding its recalcitrance response in terms of thermal degradation which in turn is a function of chemical composition and its spatial distribution.

A clear trend can be established in terms of the recalcitrance of the four groups identified in this study as analyzed by TG and FTIR, i.e., GPII > GPI > GPIII > GPIV, since extreme behaviors are well located, for example, GPII or lignin-rich biomass presented the higher structural recalcitrance; whereas GPIV or starchy-like biomass presented the lower recalcitrance among the analyzed materials; followed by GPI or cellulosic biomass, characterized to contain crystalline polymers that increase its recalcitrance to hydrolysis as well as to thermal degradation. Group III or pectin-like biomasses, in which structural recalcitrance was controlled by the bonds between polysaccharides and lignin, were classified as intermediate recalcitrance biomasses.

Table 2 shows the physicochemical characteristics of these four groups as well as the preliminary suggested conversions route for biofuel and added value products. GPII biomasses or lignin-like type do not necessarily contain a

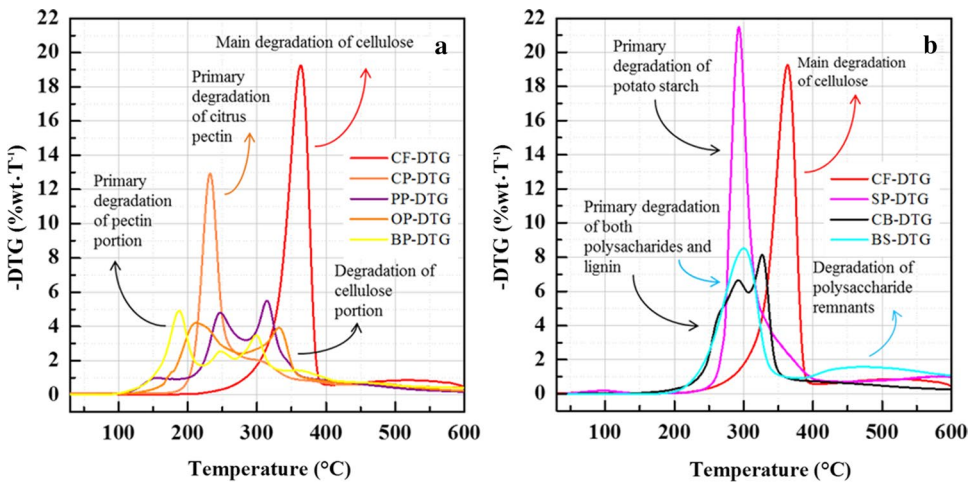

Fig. 8 DTG curves of samples of GPIII and GPIV

Table 2 Recalcitrant characteristics of GPI–GPIV biomasses and preliminary processing route selected

Group/reference biomass	Main physicochemical characteristics	Conversion route	Main added-value products
GPII/Lignin-like biomass Lignin Agave bagasse	High lignin content and high cross-linking to polysaccharides Highest recalcitrance	(1) Chemical extraction of lignin followed by (2a) Catalytic hydro processing or (2b) Thermochemical processing	Aromatic hydrocarbons (Wang et al. 2012) Biochar Precursor for carbon fiber synthesis (Mainka et al. 2015)
GPI/Cellulosic biomass Cotton fiber Sugarcane bagasse Sawdust	High degree of polymerization, high crystallinity, intermediate lignin content High recalcitrance	(1) Pre-treatment: size reduction/milling, followed by (2a) Acid treatment for hemicellulose elimination Followed by basic treatment for lignin elimination (3a) Enzymatic saccharification and fermentation or (3b) Thermochemical processing, Pyrolysis Gasification	Bioethanol (Ouyang et al. 2019) Biomaterials (Feng et al. 2018; Khoo et al. 2018) Bioethanol and cellulose (Candido et al. 2019, Beig et al. 2020) Bio-oil (Treedet and Suntivarakorn 2018) Syngas (Raheem et al. 2019)
GPIII/Pectin-like biomass Citrus pectin Banana peel Orange peel Pine apple	Intermediate recalcitrance	(1) Thermal pre-treatment followed by (2a) Acid or enzymatic hydrolysis and fermentation And (3a) Anaerobic digestion or (2b) Thermochemical processing Pyrolysis Gasification	Bioethanol (De la Torre et al. 2019, Prakash et al. 2018) Biogas (Ortiz-Sanchez et al. 2020) Bio-oil (Ozbay et al. 2019) Syngas (He et al. 2020)
GPIV/Starch-like biomass Potato starch Corn cob Barley straw	Starch-like thermal and chemical response Lower recalcitrance	(1) Basic pre-treatment (2) Acid or enzymatic hydrolysis and (3) Fermentation	Bioethanol (Boonchuay et al. 2018; Sewsynker-Sukai and Gueguim Kana 2018, Ibarra-Díaz et al. 2020)

high weight percentage of lignin, and their recalcitrance can be related to the chemical linking between polysaccharides and lignin of AB. For these biomasses, exhibiting a thermal degradation similar to LG, it is suggested a route where lignin can be extracted as a first step to maximize valorization alternatives (Wang et al. 2012), whether oriented to bioethanol obtaining or via thermochemical processing (Mainka et al. 2015).

On the other hand, GPI type or cellulosic biomasses were found to produce polyaromatic structures in their pyrolysis residue and their recalcitrance response was more similar to CF. Thus for this kind of biomass, acid solubilization of hemicellulose followed by an alkaline treatment for lignin elimination is suggested as a general conversion route towards cellulose obtaining whether for bioethanol production or biomaterial obtaining; accordingly to the best alternative identified previously for SB (Feng et al. 2018, Ouyang et al. 2019, Candido et al. 2019, Khoo et al. 2018, Beig et al. 2020). Although it is also possible to process SB through a thermochemical route to obtain bio-oil or syngas (Osorio 2019), this path is less developed in terms of added-value products.

For the GPI and GPII biomasses, a significant difference in acid/enzymatic hydrolysis yield, under similar conditions of pre-treatment, would be expected. In fact, this behavior has been confirmed by previous experimental results. For example, between SB and AB hydrolysis yield, a difference of approximately 20–30% has been reported (Hernández-Salas et al. 2009).

GPIII biomasses, PP, OP and BP, were classified as pectin-like type. Thus, a pectin extraction step followed by hydrolysis of remaining polysaccharides would be suitable towards bioethanol obtaining as previously reported for OP residue (De la Torre et al. 2019). Solid residue from pectin extraction could be treated similarly to GPI biomasses. Still, the possibility of milder process conditions is identified since its structural recalcitrance under pyrolysis conditions was lower than GPI kind. Thus, bio-oil (Ozbay et al. 2019) and syngas obtaining (He et al. 2020) is possible for these kinds of residues. It is also possible to use pectin extraction residue for biomethane production via anaerobic digestion (Ortiz-Sanchez et al. 2020).

GPIV biomasses presented the lowest recalcitrance among the twelve samples examined. Its thermal response was classified as starchy-like, and thus, acid hydrolysis or even saccharification–fermentation route could be used to obtain bioethanol (Boonchuay et al. 2018; Sewsynker-Sukai and Gueguim Kana 2018). In addition, it has been reported that basic pre-treatment for BS biomass permits the separation of lignin from hydrolyzable polysaccharides to maximize bioethanol yield (Ibarra-Díaz et al. 2020, Paschos et al. 2020), so the same treatment could be applied to CB biomass.

This latter aspect is also an advantage to group biomasses by recalcitrance similarity, since once that optimal treatment conditions have been identified for one element of the group, the same can be applied to others.

Conclusion

In this work, the recalcitrance of twelve lignocellulosic biomasses was assessed using PCA based on thermogravimetry and FTIR spectroscopy data. Four of the materials corresponding to well-known chemical composition domains were taken as reference LCB to classify the recalcitrance response of the remaining biomasses. The results from PCA analysis show that the eight different residual biomass samples can be classified into four distinct groups (GPI–GPIV) according to their thermal stability or structural recalcitrance similarity. GPII or lignin-like biomasses (LG and AB) were assessed as the most recalcitrant biomass type (devolatilization temperature: ~ 150 °C, remaining weights > 30 wt%), followed by GPI or cellulosic-like biomass (CF, SW and SB), (devolatilization temperature: 200–380 °C, remaining weights < 20 wt%). GPIII or pectin-like biomasses were classified as intermediated recalcitrance matter (CP, PP, OP, BP) (devolatilization temperature: 150–350 °C, remaining weights < 30%wt,). Finally, GPIV or starchy-like biomasses (PS, BS and CB) were the least recalcitrant among the analyzed materials (devolatilization temperature: 250–350 °C, remaining weights < 30 wt%).

GPIII and GPIV biomasses such as orange, banana peel, corn cob and barley straw presented the highest potential as a source for bioethanol production. In contrast, GPI biomasses are likely to have a better yield for cellulose biomaterials under mild conditions. GPII biomasses have the lowest potential for liquid biofuels. A better alternative for these biomasses could be biochar production as an agriculture input or as a lignin source.

This methodology could help to classify novel uncharacterized lignocellulosic biomasses based on the similarity of their recalcitrance response regarding reference materials and to preselect the processing route to obtain liquid biofuels or biomaterials in a fast and economical manner.

Supplementary Information The online version contains supplementary material available at https://doi.org/10.1007/s13762-021-03309-y.

Acknowledgements The authors wish to thank all who assisted in conducting this work.

References

Abidi N, Hequet E, Ethridge D (2007) Thermogravimetric analysis of cotton fibers: relationship with maturity and fineness. J Appl Polym Sci 103:3476–3482

Abidi N, Cabrales L, Hequet E (2010a) Thermogravimetric analysis of developing cotton fibers. Thermochim Acta 498:27–32

Abidi N, Cabrales L, Hequet E (2010b) Fourier transform infrared spectroscopic approach to the study of the secondary cell wall development in cotton fiber. Cellulose 17:309–320

Abidi N, Cabrales L, Haigler CH (2014) Changes in the cell wall and cellulose content of developing cotton fibers investigated by FTIR spectroscopy. Carbohydr Polym 100:9–16

Aburto J, Moran M, Galano A, Torres-García E (2015) Non-isothermal pyrolysis of pectin: a thermochemical and kinetic approach. J Anal Appl Pyrolysis 112:94–104

Al-Battashi HS, Annamalai N, Sivakumar N et al (2019) Lignocellulosic biomass (LCB): a potential alternative biorefinery feedstock for polyhydroxyalkanoates production. Rev Environ Sci Biotechnol 18:183–205

Anwar Z, Gulfraz M, Irshad M (2014) Agro-industrial lignocellulosic biomass a key to unlock the future bio-energy: a brief review. J Rad Res Appl Sci 7(2):163–173

Ballice L, Sert M, Saglam M, Yüksel M (2020) Determination of pyrolysis kinetics of cellulose and lignin fractions isolated from selected Turkish biomasses. Arab J Sci Eng 45(9):7429–7444

Bar-On YM, Phillips R, Milo R (2018) The biomass distribution on Earth. Proc Natl Acad Sci 115(25):6506–6511

Beig, B., Riaz, M., Naqvi, S. R., Hassan, M., Zheng, Z., Karimi, K., ... & Chi, N. T. L. (2020). Current challenges and innovative developments in pre-treatment of lignocellulosic residues for biofuel production: A Review. Fuel, 119670.

Boonchuay P, Techapun C, Leksawasdi N, Seesuriyachan P, Hanmoungjai P, Watanabe M, Chaiyaso T (2018) An integrated process for xylooligosaccharide and bioethanol production from corncob. Biores Technol 256:399–407

Brebu M, Tamminen T, Spiridon I (2013) Thermal degradation of various lignins by TG-MS/FTIR and Py-GC-MS. J Anal Appl Pyrolysis 104:531–539

Brillard A, Habermacher D, Brilhac JF (2017) Thermal degradations of used cotton fabrics and of cellulose: kinetic and heat transfer modeling. Cellulose 24:1579–1595

Cabrales L, Abidi N (2010) On the thermal degradation of cellulose in cotton fibers. J Therm Anal Calorim 102:485–491

Candido RG, Gonçalves AR (2019) Evaluation of two different applications for cellulose isolated from sugarcane bagasse in a biorefinery concept. Ind Crops Prod 142:111616

Carrier M, Loppinet-Serani A, Denux D et al (2011) Thermogravimetric analysis as a new method to determine the lignocellulosic composition of biomass. Biomass Bioenerg 35:298–307

Carrillo-Nieves D, Alanís MJR, de la Cruz Quiroz R, Ruiz HA, Iqbal HM, Parra-Saldívar R (2019) Current status and future trends of bioethanol production from agro-industrial wastes in Mexico. Renewa Sustain Energy Rev 102:63–74

Chung C, Lee M, Choe EK (2004) Characterization of cotton fabric scouring by FT-IR ATR spectroscopy. Carbohydr Polym 58:417–420

De la Torre I, Martin-Dominguez VICTOR, Acedos MG, Esteban J, Santos VE, Ladero MIGUEL (2019). Utilisation/upgrading of orange peel waste from a biological biorefinery perspective. Appl Microbiol Biotechnol 103(15):5975–5991

De Palma KR, García-Hernando N, Silva MA et al (2019) Pyrolysis and combustion kinetic study and complementary study of ash fusibility behavior of sugarcane bagasse, sugarcane straw, and their pellets: case study of agro-industrial residues. Energy Fuels 33:3227–3238

Dhyani V, Bhaskar T (2018) A comprehensive review on the pyrolysis of lignocellulosic biomass. Renew Energy 129:695–716

Einhorn-Stoll U, Kunzek H, Dongowski G (2007) Thermal analysis of chemically and mechanically modified pectins. Food Hydrocoll 21:1101–1112

Feng YH, Cheng TY, Yang WG, Ma PT, He HZ, Yin XC, Yu XX (2018) Characteristics and environmentally friendly extraction of cellulose nanofibrils from sugarcane bagasse. Ind Crops Prod 111:285–291

Fisher T, Hajaligol M, Waymack B, Kellogg D (2002) Pyrolysis behavior and kinetics of biomass derived materials. J Anal Appl Pyrolysis 62:331–349

García R, Pizarro C, Lavín AG, Bueno JL (2013) Biomass proximate analysis using thermogravimetry. Bioresour Technol 139:1–4

Gil MV, González-Vázquez MP, García R, Rubiera F, Pevida C (2019) Assessing the influence of biomass properties on the gasification process using multivariate data analysis. Energy Conv Manage 184:649–660

Giummarella N, Pu Y, Ragauskas AJ, Lawoko M (2013) A critical review on the analysis of lignin carbohydrate bonds. Green Chem 21:23

He J, Yang Z, Xiong S, Guo M, Yan Y, Ran J, Zhang L (2020) Experimental and thermodynamic study of banana peel non-catalytic gasification characteristics. Waste Manage 113:369–378

Hersh SP, Carolina N, Mark HF (2006) Cotton Fiber Chemistry and Technology, 1st. edn. Taylor & Francis Group, LLC

Hernández-Salas JM, Villa-Ramírez MS, Veloz-Rendón JS, Rivera-Hernández KN, González-César RA, Plascencia-Espinosa MA, Trejo-Estrada SR (2009) Comparative hydrolysis and fermentation of sugarcane and agave bagasse. Bioresour Technol 100(3):1238–1245

Huang Y, Wang L, Chao Y et al (2012) Analysis of lignin aromatic structure in wood based on the IR spectrum. J Wood Chem Technol 32:294–303

Ibarra-Díaz N, Castañón-Rodríguez JF, Gómez-Rodríguez J, Aguilar-Uscanga MG (2020) Optimization of peroxide-alkaline pretreatment and enzymatic hydrolysis of barley straw (*Hordeum vulgare* L.) to produce fermentable sugars using a Box–Behnken design. Biomass Conv Bioref 1–10

Karimi K, Taherzadeh MJ (2016) A critical review of analytical methods in pre-treatment of lignocelluloses: Composition, imaging, and crystallinity. Bioresour Technol 200:1008–1018

Kawamoto H (2017) Lignin pyrolysis reactions. J Wood Sci 63:117–132

Khoo RZ, Chow WS, Ismail H (2018) Sugarcane bagasse fiber and its cellulose nanocrystals for polymer reinforcement and heavy metal adsorbent: a review. Cellulose 25(8):4303–4330

Lazzari E, Schena T, Marcelo MCA, Primaz CT, Silva AN, Ferrão MF, Caramão EB (2018) Classification of biomass through their pyrolytic bio-oil composition using FTIR and PCA analysis. Ind Crops Prod 111:856–864

Lemos PVF, Barbosa LS, Ramos IG, Coelho RE, Druzian JI (2019) Characterization of amylose and amylopectin fractions separated from potato, banana, corn, and cassava starches. Int J Biol Macromol 132:32–42

Liang J, Chen J, Wu S et al (2018) Comprehensive insights into cellulose structure evolution: via multi-perspective analysis during a slow pyrolysis process. Sustain Energy Fuels 2:1855–1862

Lin YC, Cho J, Tompsett GA et al (2009) Kinetics and mechanism of cellulose pyrolysis. J Phys Chem C 113:20097–20107

Liu X, Yu L, Xie F et al (2010) Kinetics and mechanism of thermal decomposition of cornstarches with different amylose/amylopectin ratios. Starch/Staerke 62:139–146

Liu Y, He Z, Shankle M, Tewolde H (2016) Compositional features of cotton plant biomass fractions characterized by attenuated total reflection Fourier transform infrared spectroscopy. Ind Crops Prod 79:283–286

Lupoi JS, Singh S, Simmons BA, Henry RJ (2014) Assessment of lignocellulosic biomass using analytical spectroscopy: an evolution to high-throughput techniques. Bioenergy Res 7:1–23

Mainka H, Täger O, Körner E, Hilfert L, Busse S, Edelmann FT, Herrmann AS (2015) Lignin–an alternative precursor for sustainable and cost-effective automotive carbon fiber. J Market Res 4(3):283–296

Melati RB, Shimizu FL, Oliveira G, Pagnocca FC, de Souza W, Sant'Anna C, Brienzo M (2019) Key factors affecting the recalcitrance and conversion process of biomass. BioEnergy Res 12(1):1–20

Mishra RK, Mohanty K (2018a) Pyrolysis kinetics and thermal behavior of waste sawdust biomass using thermogravimetric analysis. Bioresour Technol 251:63–74

Mishra RK, Mohanty K (2018b) Characterization of non-edible lignocellulosic biomass in terms of their candidacy towards alternative renewable fuels. Biomass Conv Bioref 8(4):799–812

Munir S, Daood SS, Nimmo W et al (2009) Thermal analysis and devolatilization kinetics of cotton stalk, sugar cane bagasse and shea meal under nitrogen and air atmospheres. Bioresour Technol 100:1413–1418

Olatunji, O. O., Akinlabi, S. A., Mashinini, M. P., Fatoba, S. O., & Ajayi, O. O. (2018). Thermo-gravimetric characterization of biomass properties: a review. In IOP Conf. Ser. Mater. Sci. Eng (Vol. 423, No. 1, p. 012175).

Ortiz-Sanchez M, Solarte-Toro JC, Orrego-Alzate CE, Acosta-Medina CD, Cardona-Alzate CA (2020) Integral use of orange peel waste through the biorefinery concept: an experimental, technical, energy, and economic assessment. Biom Conv Biorefin 11(2):645–659

Osorio J, Chejne F (2019) Bio-oil production in fluidized bed reactor at pilot plant from sugarcane bagasse by catalytic fast pyrolysis. Waste Biomass Valor 10:187–195

Ouyang S, Qiao H, Xu Q et al (2019) Development of two-step pre-treatment of Chinese fir sawdust using dilute sulfuric acid followed by sodium chlorite for bioethanol production. Cellulose 26:8513–8524

Ozbay N, Yargic AS, Sahin RZY, Yaman E (2019) Valorization of banana peel waste via in-situ catalytic pyrolysis using Al-Modified SBA-15. Ren Energy 140:633–646

Park CW, Youe WJ, Namgung HW, Han SY, Seo PN, Chae HM, Lee SH (2018) Effect of lignocellulose nanofibril and polymeric methylene diphenyl diisocyanate addition on plasticized lignin/polycaprolactone composites. BioResources 13(3):6802–6817

Paschos T, Louloudi A, Papayannakos N, Kekos D, Mamma D (2020) Potential of barley straw for high titer bioethanol production applying pre-hydrolysis and simultaneous saccharification and fermentation at high solid loading. Biofuels 1–7

Pereira SC, Maehara L, Machado CMM, Farinas CS (2016) Physical-chemical-morphological characterization of the whole sugarcane lignocellulosic biomass used for 2G ethanol production by spectroscopy and microscopy techniques. Renew Energy 87:607–617

Prakash H, Chauhan PS, General T, Sharma AK (2018) Development of eco-friendly process for the production of bioethanol from banana peel using inhouse developed cocktail of thermo-alkali-stable depolymerizing enzymes. Bioprocess Biosyst Eng 41(7):1003–1016

Raheem A, Zhao M, Dastyar W, Channa AQ, Ji G, Zhang Y (2019) Parametric gasification process of sugarcane bagasse for syngas production. Int J Hydrogen Energy 44(31):16234–16247

Rajendran NS, Thampi H (2019) Extraction and characterisation of pectin from banana peel. Carpathian J Food Sci Technol 11(4)

Ramezani N, Sain M (2018) Thermal and physiochemical characterization of lignin extracted from wheat straw by organosolv process. J Polym Environ 26(7):3109–3116

Rios M, Kaltschmitt M (2013) Bioenergy potential in Mexico—status and perspectives on a high spatial distribution. Biomass Conv Bioref 3(3):239–254

Rodier L, Bilba K, Onésippe C, Arsène MA (2019) Utilization of bio-chars from sugarcane bagasse pyrolysis in cement-based composites. Ind Crops Prod 141:111731

Rudnik E, Matuschek G, Milanov N, Kettrup A (2006) Thermal stability and degradation of starch derivatives. J Therm Anal Calorim 85:267–270

Santoni I, Callone E, Sandak A et al (2015) Solid state NMR and IR characterization of wood polymer structure in relation to tree provenance. Carbohydr Polym 117:710–721

Sewsynker-Sukai Y, Kana EG (2018) Simultaneous saccharification and bioethanol production from corn cobs: Process optimization and kinetic studies. Biores Technol 262:32–41

Shah MA, Khan MNS, Kumar V (2018) Biomass residue characterization for their potential application as biofuels. J Therm Anal Calorim 134(3):2137–2145

Tovar AK, Godínez LA, Espejel F, Ramírez-Zamora RM, Robles I (2019) Optimization of the integral valorization process for orange peel waste using a design of experiments approach: Production of high-quality pectin and activated carbon. Waste Manage 85:202–213

Treedet W, Suntivarakorn R (2018) Design and operation of a low cost bio-oil fast pyrolysis from sugarcane bagasse on circulating fluidized bed reactor in a pilot plant. Fuel Process Technol 179:17–31

Valdez-Vazquez I, Acevedo-Benítez JA, Hernández-Santiago C (2010) Distribution and potential of bioenergy resources from agricultural activities in Mexico. Ren Sustain Energy Rev 14:2147–2153

Wang Y, He T, Liu K, Wu J, Fang Y (2012) From biomass to advanced bio-fuel by catalytic pyrolysis/hydro-processing: Hydrodeoxygenation of bio-oil derived from biomass catalytic pyrolysis. Biores Technol 108:280–284

Xin S, Yang H, Chen Y et al (2015) Chemical structure evolution of char during the pyrolysis of cellulose. J Anal Appl Pyrolysis 116:263–271

Xu F, Yu J, Tesso T et al (2013) Qualitative and quantitative analysis of lignocellulosic biomass using infrared techniques : a mini review. Appl Energy 104:801–809

Yang H, Yan R, Chen H et al (2007) Characteristics of hemicellulose, cellulose and lignin pyrolysis. Fuel 86:1781–1788

Yang H, Yan R, Chen H et al (2011) In-Depth Investigation of biomass pyrolysis based on three major components: Hemicellulose, cellulose, and lignin. Ind Eng Chem Res 50:10424–10433

Zhao X, Zhang L, Liu D (2012) Biomass recalcitrance. Part I: the chemical compositions and physical structures affecting the enzymatic hydrolysis of lignocellulose. Biofuels Bioprod Biorefin 6(4):465–482

Zhao S, Liu M, Zhao L, Zhu L (2018) Influence of interactions among three biomass components on the pyrolysis behavior. Ind Eng Chem Res 57:5241–5249

Zoghlami A, Paës G (2019) Lignocellulosic biomass: understanding recalcitrance and predicting hydrolysis. Front Chem 7:874